ISSN 1674-1056
http://cpb.iphy.ac.cn
http://iopscience.iop.org/cpb
中国物理 B
Chinese Physics
中国物理 Chinese Physics B

Theoretical analysis of cross-plane lattice thermal conduction in graphite

Yun-Feng Gu(顾云风)

Citation: Chin. Phys. B . 2019, 28(6): 066301. **doi:** 10.1088/1674-1056/28/6/066301
Journal homepage: http://cpb.iphy.ac.cn; http://iopscience.iop.org/cpb

What follows is a list of articles you may be interested in

Thermal transport in phosphorene and phosphorene-based materials: A review on numerical studies

Yang Hong(洪扬), Jingchao Zhang(张景超), Xiao Cheng Zeng(曾晓成)
Chin. Phys. B . 2018, 27(3): 036501. **doi:** 10.1088/1674-1056/27/3/036501

First-principles calculations of structural and thermodynamic properties of *β*-PbO

Vahedeh Razzazi, Sholeh Alaei
Chin. Phys. B . 2017, 26(11): 116501. **doi:** 10.1088/1674-1056/26/11/116501

Lattice stabilities, mechanical and thermodynamic properties of Al_3Tm and Al_3Lu intermetallics under high pressure from first-principles calculations

Xu-Dong Zhang(张旭东) and Wei Jiang(姜伟)
Chin. Phys. B . 2016, 25(2): 026301. **doi:** 10.1088/1674-1056/25/2/026301

High-pressure phonon dispersion of copper by using the modified analytic embedded atom method

Zhang Xiao-Jun, Chen Chang-Le, Feng Fei-Long
Chin. Phys. B . 2013, 22(9): 096301. **doi:** 10.1088/1674-1056/22/9/096301

Lattice dynamical and thermodynamical properties of ReB_2, RuB_2, and OsB_2 compounds in the ReB_2structure

E. Deligoz, K. Colakoglu, Y. O. Ciftci
Chin. Phys. B . 2012, 21(10): 106301. **doi:** 10.1088/1674-1056/21/10/106301

Theoretical analysis of cross-plane lattice thermal conduction in graphite*

Yun-Feng Gu(顾云风)†

College of Electronic and Mechanical Engineering, Nanjing Forestry University, Nanjing 210037, *China*

(Received 7 March 2019; revised manuscript received 27 March 2019; published online 8 May 2019)

A theoretical analysis of the cross-plane lattice thermal conduction in graphite is performed by using first-principles calculations and in the single-mode relaxation time approximation. The out-of-plane phonon acoustic mode ZA and optical mode ZO′ have almost 80% and 20% of contributions to cross-plane heat transfer, respectively. However, these two branches have a small part of total specific heat above 300 K. Phonons in the central 16% of Brillouin zone contribute 80% of cross-plane transport. If the group velocity angle with respect to the graphite layer normal is less than 30°, then the contribution is 50% at 300 K. The ZA phonons with long cross-plane mean free path are focused in the cross-plane direction, and the largest mean free path is on the order of several micrometers at room temperature. The average value of cross-plane mean free path at 300 K is 112 nm for ZA phonons with group velocity angle with respect to the layer normal being less than 15°. The average value is dropped to 15 nm when phonons of all branches in the whole Brillouin zone are taken into account, which happens because most phonons have small or even no contributions.

Keywords: graphite, cross-plane thermal conduction, phonon mean free path, layered systems

PACS: 63.20.D–, 63.22.Np, 65.40.–b **DOI:** 10.1088/1674-1056/28/6/066301

1. Introduction

Graphite is composed of many graphene monolayers, where carbon atoms in the layer are arranged into a hexagonal lattice connected by strong covalent bonds and only weak Van der Waals (vdW) force exists between layers. The study of phonon cross-plane (CP) thermal conduction in graphite is helpful in revealing the phonon transport mechanism in vdW layered material in the vertical direction[1] or across the vdW interface between individual nanostructures or nanostructure and substrate/host material.[2]

It is generally accepted that graphite has a very low CP thermal conductivity. The measurements[3,4] performed decades ago already showed that the graphite CP thermal conductivity is only about 7 W/mK. However, there are still many debates about the mechanism of phonon CP transfer. For example, the average values of mean free path (MFP) in CP direction Λ_c are significantly different in different models. In the classic kinetic theory based on an isotropic assumption, Λ_c is less than one nanometer in Ref. [5], and about 6.7 nm in Ref. [6]. As a comparison, Sadeghi *et al.*[7] performed a calculation by using the full phonon dispersion of graphite based on the density functional perturbation theory, and estimated Λ_c at 20 nm under 300 K. In the molecular dynamics simulation, Λ_c is on the order of several hundred nanometers.[8] Harb *et al.*[9] measured a CP thermal conductivity of a graphite thin film to be 35 nm by time resolved x-ray diffraction, and reported a value of about 0.7 W/mK much lower than the value of bulk graphite, which suggests that MFP in CP direction can be longer than 35 nm. Fu *et al.*[10] measured the CP thermal conductivity of thin graphite flakes with different thickness values by using a differential three-omega method, and then estimated Λ_c at around 200 nm at room temperature. In a similar experiment carried out by Zhang *et al.*,[11] through using the time-domain thermoreflectance technique, Λ_c is found to be a few hundred nanometers at room temperature and a much narrower distribution than in isotropic crystals. It should be noted that MFP cannot be measured directly but it can be estimated by the MFP reconstruction method to link the measured thermal conductivities to the MFP spectrum.[12,13] However, this is a challenging problem because different MFP spectra may lead to the same thermal conductivity.

According to the experimental measurements, Yang *et al.*[14] suggested that the high frequency phonons can propagate only in the basal plane but not in the CP direction because of the weak vdW interaction between basal planes. Therefore, these high frequency phonons should not be included in the calculation, and, as a result, Λ_c could be over 100 nm at room temperature. Recently, a similar idea is found in the work of Han *et al.*[15] on the assumption that high frequency phonons are confined in the graphite layer, and have to exchange energy with the low-frequency phonons under 4 THz which are the only phonons allowed to transfer in the CP direction. Furthermore, taking into account only a small part of volumetric heat capacity contributed from these low frequency phonons, they predict a *c*-axis MFP of 165 nm at 300 K based on a mod-

*Project supported by the National Natural Science Foundation of China (Grant No. 51376094) and Jiangsu Overseas Visiting Scholar Program for University Prominent Young & Middle-aged Teachers and Presidents.

†Corresponding author. E-mail: gu_yunfeng@sina.com

© 2019 Chinese Physical Society and IOP Publishing Ltd

ified one-dimensional kinetic theory.

There are still many controversies and debates about the contributions from different phonon modes. In this paper, we will give a wave vector and polarization/branch resolved analysis of all the phonon modes in Brillouin zone (BZ) directly, with the help of the almaBTE first-principles phonon solver.[16] The rest of this paper is organized as follows. In Section 2, the method used in the calculation is briefly given. In Section 3, we calculate the phonon dispersion, thermal conductivity and specific heat at constant volume, including a comparison with measurements to make sure that we have a good starting point. The CP thermal conductivity, specific heat and MFP of different branches in different part of BZ are then analyzed. Finally, some conclusions are drawn from the present study.

2. Methods

Under the relaxation time approximation (RTA) and in the framework of Boltzmann transport equation, the CP thermal conductivity can be expressed as[17]

$$\kappa = \frac{1}{(2\pi)^3}\sum_p \int_{\mathrm{BZ}} \left\{v_{p\boldsymbol{q}}\right\}_{\mathrm{c}}^2 \tau_{p\boldsymbol{q}} C_{p\boldsymbol{q}}\,\mathrm{d}\boldsymbol{q}, \tag{1}$$

and the specific heat at constant volume can be obtained from the sum of specific heat per mode $C_{p\boldsymbol{q}}$, and defined as[17]

$$C = \frac{1}{(2\pi)^3}\sum_p \int_{\mathrm{BZ}} C_{p\boldsymbol{q}}\,\mathrm{d}\boldsymbol{q} = \frac{1}{(2\pi)^3}\sum_p \int_{\mathrm{BZ}} k_{\mathrm{B}} \frac{x^2 \mathrm{e}^x}{(\mathrm{e}^x-1)^2}\,\mathrm{d}\boldsymbol{q},$$
$$x = \hbar\omega_{p\boldsymbol{q}}/k_{\mathrm{B}}T, \tag{2}$$

where p and $\boldsymbol{q}$ denote, respectively, the phonon polarization and wave vector, $\left\{v_{p\boldsymbol{q}}\right\}_{\mathrm{c}}$ is the velocity component in the CP direction, $\hbar$ is the reduced Planck constant, $\omega_{p\boldsymbol{q}}$ is the phonon frequency, k_{B} is the Boltzmann constant, and T is the temperature. The total scattering rate can be calculated based on Matthiessen's rule $1/\tau_{p\boldsymbol{q}} = 1/\tau^{+}_{p\boldsymbol{q}} + 1/\tau^{-}_{p\boldsymbol{q}}$, where the three-phonon scattering rates $1/\tau^{+}_{p\boldsymbol{q}}$ and $1/\tau^{-}_{p\boldsymbol{q}}$ correspond to absorption process and emission process, respectively.[17] In this work, we limit the consideration of scattering phenomena to these two kinds of three-phonon inelastic scatterings. The MFP of mode $p\boldsymbol{q}$ can be defined in terms of the total phonon relaxation time $\tau_{p\boldsymbol{q}}$ as $\Lambda_{p\boldsymbol{q}} = \left|v_{p\boldsymbol{q}}\right|\tau_{p\boldsymbol{q}}$, and MFP in the CP direction can be defined as[16]

$$\left\{\Lambda_{p\boldsymbol{q}}\right\}_{\mathrm{c}} = \left|\left\{v_{p\boldsymbol{q}}\right\}_{\mathrm{c}}\right|\tau_{p\boldsymbol{q}}. \tag{3}$$

The average MFP in the CP direction Λ_{c} can be calculated from[7]

$$\Lambda_{\mathrm{c}}^{-1} = \frac{1}{\kappa}\frac{1}{(2\pi)^3}\sum_p \int_{\mathrm{BZ}} \left|\left\{v_{p\boldsymbol{q}}\right\}_{\mathrm{c}}\right| C_{p\boldsymbol{q}}\,\mathrm{d}\boldsymbol{q}. \tag{4}$$

The precondition to obtain the phonon thermal conduction is to acquire the phonon dispersion relation $\omega_{p\boldsymbol{q}}$ and the anharmonic phonon-phonon scattering rate $1/\tau^{\pm}_{p\boldsymbol{q}}$, which involve the calculation of second- and third-order interatomic force constants (IFCs). The calculation in this paper is performed using the almaBTE first-principles phonon solver.[16] The IFCs used in this paper for graphite are taken from the online almaBTE database,[18] the corresponding supercells are $7\times7\times3$, and the cutoff of 10th nearest neighbors is introduced during the calculation of the third-order IFCs.

The integrations in Eqs. (1), (2), and (4) run over the entire BZ of bulk graphite crystal, which is hexagonal, as shown in Fig. 1. In the almaBTE package,[16] the BZ is discretized into a regular wave vector grids, denoted by green dots in Fig. 1. There are $N = N_1\times N_1\times N_2$ grids with N_1 denoting the in-plane (IP) direction and N_2 the CP direction. Each grid contains a small volume fraction of the BZ, and has a wave vector $\boldsymbol{q}$, frequency $\omega_{p\boldsymbol{q}}$ for the phonon polarization p according to the phonon dispersion relation. With the almaBTE package, we can furthermore show the distributions of many physical quantities, such as relaxation time $\tau_{p\boldsymbol{q}}$, specific heat $C_{p\boldsymbol{q}}$, thermal conductivity, *etc*. in the wave vector grids. Hence the integration over BZ is transformed into summations over all phonon polarizations and wave vector grids. The wave vector grid of $36\times36\times12$ as illustrated in Fig. 1 is used to fulfill the convergence requirements of $1/\tau^{\pm}_{p\boldsymbol{q}}$ and κ.

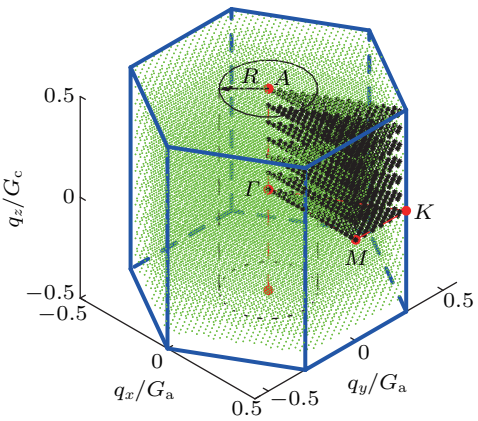


Fig. 1. Schematic illustration of BZ of graphite with wave vector grids denoted by green dots. The black dots refer to the irreducible wave vector grids. G_{a} and G_{c} denote length of reciprocal-lattice vector along the plane and CP direction, respectively. R is radius of a cylinder with axis coinciding with Γ–A. The cylinder is used to choose phonon modes in the center of BZ.

3. Results and discussion

The calculated graphite phonon dispersion is denoted by dots in Fig. 2. The triangles, circles and squares refer to the experiment results.[19–21] These phonons are in the high-symmetry directions ΓK, ΓM, and ΓA in BZ as shown in Fig. 1. The calculated results accord well with the measurements, which presents a solid foundation for further study.

The building block of graphite is the graphene monolayer, which has two atoms per unit cell. These layers are bound to-

gether by a weak vdW force. There are six phonon branches for graphene. Each of these six branches splits into two branches for graphite which has four atoms per unit cell.[22] Therefore, graphite has twelve branches, *i.e.*, three acoustic (A) branches (LA, TA, ZA) and nine optical (O) branches. Except for ZA and ZO′, the remaining branches are double degenerate almost in the entire BZ. Herein L, T, and Z represent longitudinal polarization, in-plane and out-of-plane transversal polarization, respectively. Strictly speaking, these labels hold true only along the high-symmetry directions in BZ, such as ΓK and ΓM, and are misleading for arbitrary wave vectors. However, these labels are useful in classifying the branches. For the ZA banch and ZO′ branch denoted by lines in Fig. 2, the atoms in the graphite layers vibrate along the out-of-plane direction. These two branches are split from graphene ZA (flexural) branch, which also has out-of-plane vibrations and exhibits a quadratic dispersion near Γ[22] However, as a three-dimensional material, graphite has wave vectors which are not confined in the in-plane directions. Therefore, ZA and ZO′ are, in fact, respectively longitudinal acoustic and optical branch for phonons with wave vectors along ΓA in BZ[23], as shown in Fig. 2(b).

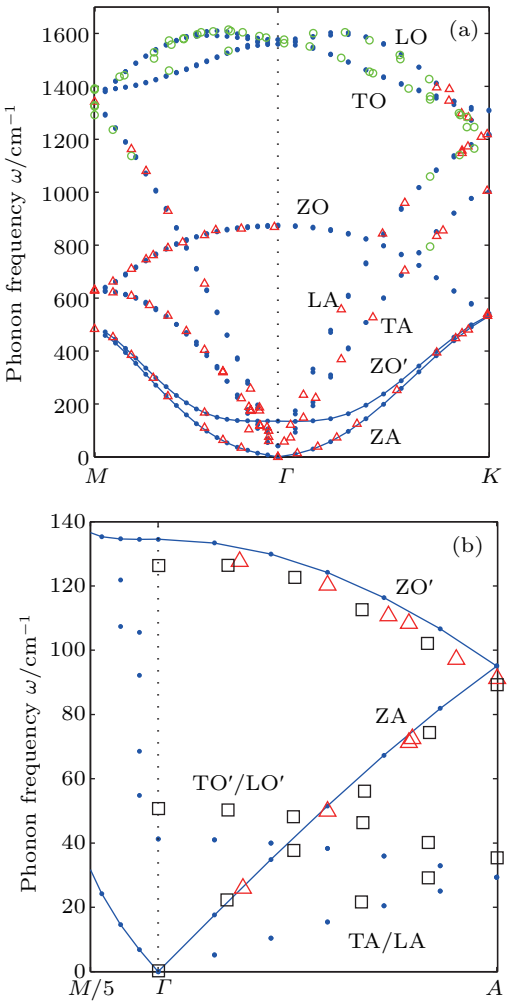


Fig. 2. Phonon dispersion in graphite along high-symmetry direction. Blue dots are for calculations. Triangles and circles are for inelastic x-ray scattering measurements from Refs. [19] and [20] respectively. Squares are for neutron scattering data from Ref. [21]. The solid lines are used to show the two branches ZA and ZO′, which are discussed in detail in this paper.

Based on the phonon dispersion over the entire BZ grids in Fig. 1, the calculated CP thermal conductivity κ_{total} represented by the line with square symbols slightly overestimates the measurement $\kappa_{\text{experiment}}$[24] denoted by triangles in Fig. 3(a) in a temperature range of 100 K–1000 K. This result is reasonable because the only scattering taken into account is the three-phonon process.

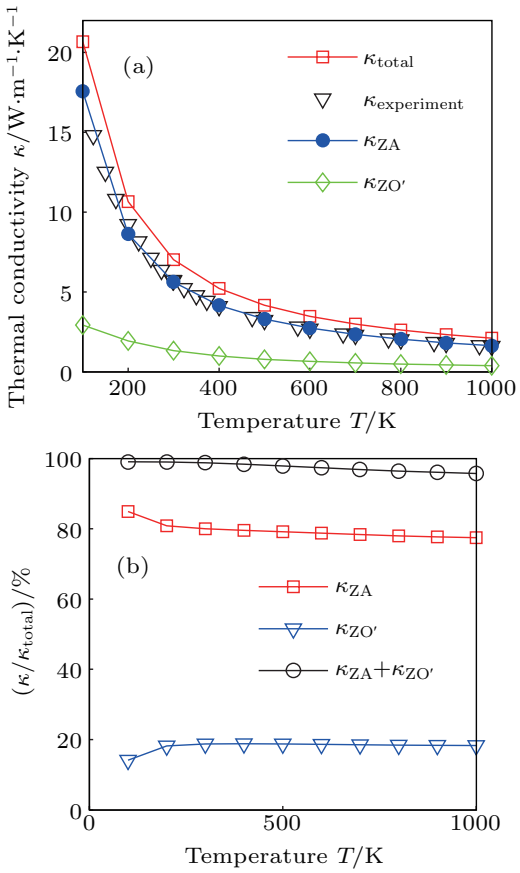


Fig. 3. (a) Comparison between CP thermal conductivity measurements (triangles)[24] and the calculated results of κ_{total} (line with squares), including its ZA and ZO′ branch contributions. (b) Temperature-dependent different phonon percentage contributions.

Although there are 12 branches, only two branches, *i.e.*, ZA and ZO′ represented by solid lines in Fig. 2, have significant contributions to CP thermal conduction, as reported by Paulatto *et al.*[22] The temperature dependence of κ_{ZA} (line with dots) and $\kappa_{\text{ZO′}}$ (line with diamonds) are illustrated in Fig. 3(a), and their percentage contributions are shown in Fig. 3(b). The sum of the partial contributions due to ZA and ZO′ phonons denoted by the line with circle is almost 100% of total thermal conductivity, and slightly decreases as temperature rises because high temperature can excite more high-frequency phonons belonging to other branches to participate in thermal conduction. From 200 K to 1000 K, about 80% and 20% of contributions come from ZA and ZO′ phonons, respectively.

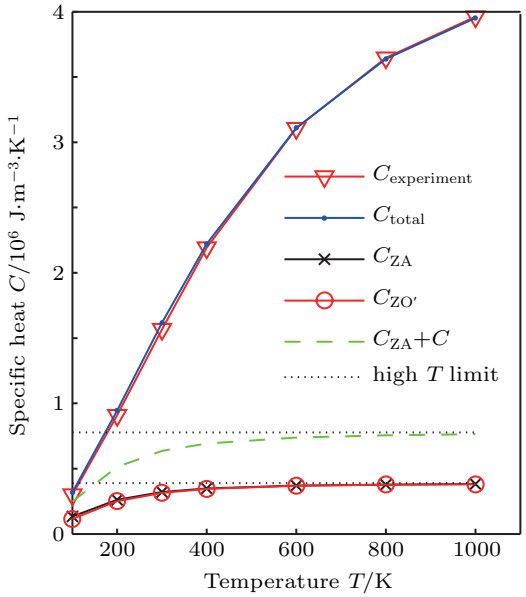


Fig. 4. Plots of specific heat at constant volume of graphite *versus* temperature. The line with dots takes into account all the branches. ZA branch and ZO′ branch and their sum are represented by line with x symbols, line with circles, and dashed line, respectively. The line with triangles is for experiment results from Ref. [25]. Dotted lines represent high-temperature limits.

Based on the phonon dispersion over the entire BZ, the specific heat at constant volume of graphite is calculated as illustrated in Fig. 4. The C_{total} (line with dots) takes into account all the branches and accords well with the experiment values (line with triangles).[25] The ZA and ZO′ branch, denote respectively by the line with x symbols and the line with circles almost have the same specific heat in a temperature range of 100 K–1000 K. The dotted lines identify the high temperature limits for different phonon branches in which each phonon mode simply contributions to the specific heat the same constant value as required by the Dulong and Petit law.[26] As illustrated in Fig. 2, the ZA and ZO′ branch each have a low maximum phonon frequency. Therefore, as temperature rises, it is easy to satisfy $x = \hbar\omega_{pq}/k_{\text{B}}T \ll 1$ which will lead to the specific heat per mode in Eq. (2) $C_{pq} = k_{\text{B}}x^2\,\mathrm{e}^x/(\mathrm{e}^x-1)^2 \approx k_{\text{B}}$. At 100 K, the ZA branch and ZO′ branch have the dominant contributions to the specific heat. A further rise in the temperature will excite more high phonons belonging to other branches, which leads to a dramatic increase in the total specific heat C_{total}, while C_{ZA} and $C_{\text{ZO}'}$ begin to approach to the high temperature limits and cannot increase significantly. This situation means that the sum of C_{ZA} and $C_{\text{ZO}'}$ represented by the dashed line in Fig. 4 can only contribute a small part of the total specific heat as temperature rises.

The results shown in Figs. 3 and 4 reveal that in the view of thermal conduction in the CP direction, except for ZA and ZO′, the remaining phonon branches occupy most of thermal energy but are trapped in graphite layers above 300 K. Polarized in the CP direction, ZA and ZO′ phonons act as the dominant interlayer thermal energy carriers. Graphite, as a vdW layered material, has a weak interaction between layers. The vdW force is sensitive to the distance between atoms. Atoms in the neighbor layers have the smallest distance with relatively strong vdW interaction, and vibrate in the CP direction to change the interatomic distance dramatically in the ZA mode and ZO′ mode. This kind of vibration can benefit the interlayer transfer of thermal energy.

The wave vector resolved plots of CP thermal conductivity of ZA branch and ZO′ branch are illustrated in Fig. 5. The results are for the irreducible wave vector grids highlighted as black dots in Fig. 1. These grids represent the discrete irreducible BZ, the smallest wedge reduced from BZ by all of the symmetries. Each grid occupies a small volume of BZ, in which phonons have contributions to CP thermal conductivity, represented by the color of dots in Fig. 5. The exact value of the contribution can change with the density of grids, or the grid volume. However, figure 5 reveals the distribution of contributions from phonons in different parts of BZ.

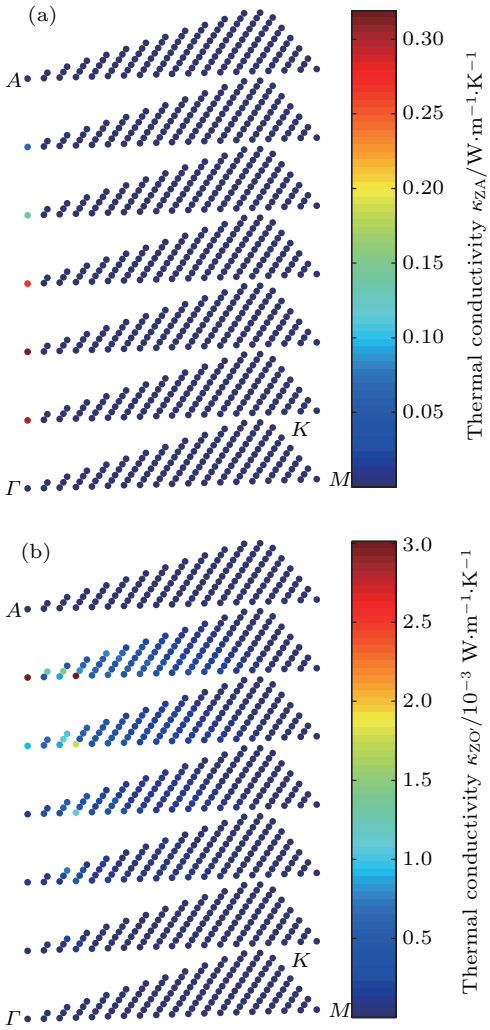


Fig. 5. Distributions of CP thermal conductivity contribution from (a) branch ZA and (b) branch ZO′ over the irreducible wave vector grids at 300 K.

For ZA branch, figure 5(a) reveals that the phonons in the grids along the Γ–A line have major contributions, and significantly larger than in the other parts of BZ. The CP thermal conductivity of ZO′ phonons has a significantly smaller value than that of ZA phonons, and is relatively evenly distributed

in the identical grids as shown in Fig. 5(b). Moreover, the ZO′ phonons in the vicinity of Γ–A line and near to point A are more likely to participate in the CP thermal conduction. It should be noted that because only a few grids have very large contributions for ZA phonons, $\kappa_{\rm ZA}$ is only about four times the value of $\kappa_{\rm ZO'}$ at 300 K as shown in Fig. 3(b).

To find which parts of phonons in BZ are critical for CP thermal conduction, a cylinder shape with its axis coinciding with Γ–A is defined in Fig. 1. The relation between the normalized cumulative CP thermal conductivity $100\% \times \kappa/\kappa_{\rm total}$ at 300 K and the cylinder radius R is illustrated in Fig. 6. The lines with circles, triangles and squares represent the case in which κ takes into account the contribution from all branch phonons, ZA phonons, and ZO′ phonons in the cylinder, respectively. When $R = 0.2G_{\rm a}$, phonons in the cylinder transfer about 80% thermal energy in the CP direction. A similar conclusion was obtained by Paulatto *et al.*[22] In addition, ZA phonons have the dominant contribution, especially when R is small. It appears that ZA phonons are the only thermal energy carriers along the Γ–A line, and contributes about 30% of the CP transport. The ZO′ phonons have significantly less contribution than ZA phonons, and the contribution is approximately proportional to the cylinder radius until it reaches its maximum value 20% at $R = 0.4G_{\rm a}$. Phonons near the edge of BZ ($R > 0.4G_{\rm a}$) have almost no contribution.

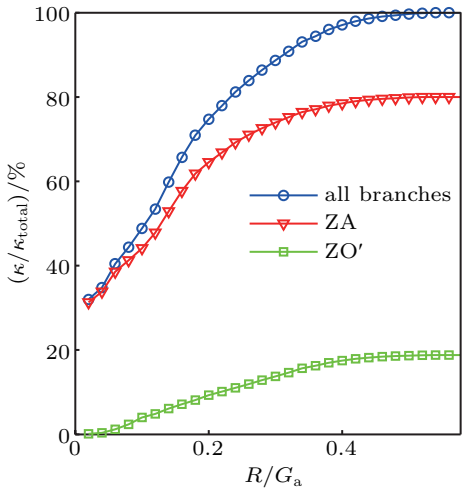


Fig. 6. Plots of normalized cumulative CP thermal conductivity at 300 K *versus* radius R of cylinder in BZ with axis coinciding with Γ–A.

Graphite is famous for its anisotropic properties. Therefore, it is reasonable to explore the direction dependence of phonon transport. Herein, we divide the entire BZ into six sectors according to the wave vector angle $\theta\,(q,z)$ (or the group velocity angle $\theta\,(v,z)$) with respect to the graphite layer normal, and assess the contribution due to phonons in these sectors. Figure 7 shows the slices of the iso-energy surfaces in the A–Γ–M plane which is divided uniformly into six sectors by the dash-dotted lines with respect to $\theta\,(q,z)$. The vertex angle of each sector at the point Γ is 15°. The arrows indicate the directions of the group velocities which are normal to the iso-energy surfaces. The length of arrows represents the velocity magnitude. There are six velocity arrow groups identified by different colors according to the angle $\theta\,(v,z)$ specified in the legend below the figure.

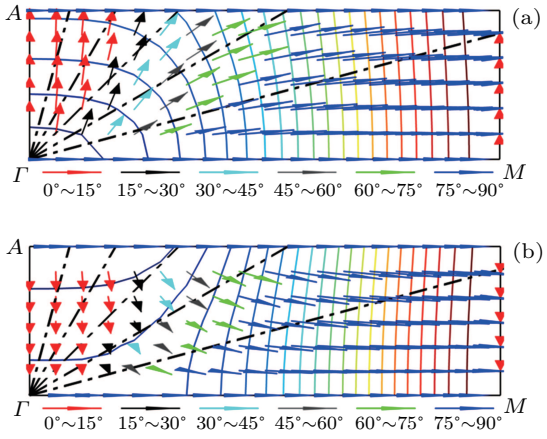


Fig. 7. Slices of the iso-energy surfaces of (a) ZA and (b) ZO′ phonon in A–Γ–M plane. The plane is divided into 6 sections by dash dotted lines. according to angle $\theta\,(q,z)$ between wave vector and Γ–A direction. Group velocities denoted by arrows are divided into 6 groups identified by different colors with legend shown below the figure according to angle $\theta\,(v,z)$ between velocity direction and Γ–A direction.

As an acoustic phonon, the ZA mode has a zero frequency at the Γ point, which is the center of an ellipsoid iso-energy surface in the low frequency range as shown in Fig. 7(a). Furthermore, the ellipsoid surface grows in the graphite flat hexagonal prism shape BZ as frequency rises, and transforms into a cylinder surface coaxial with Γ–A. As shown in Fig. 7(b), the ZO′ branch has similar iso-energy surfaces, but its lowest frequency of optical phonons is not zero and is at the A point.

The anisotropic ellipsoid shape and the cylinder shape of iso-energy surface are attributed to the strong bonding between atoms in the graphite layer accompanied with the weak vdW interaction between layers. The group velocity arrows normal to the iso-energy surfaces in Fig. 7 indicate the direction of energy flow. The anisotropic shape of iso-energy surface results in the existence of regions that each have a small curvature, where phonons tend to transfer energy in nearly the same direction, instead of along the wave vector direction. This phenomenon, especially when phonon ballistic transport plays a remarkable role at low temperature, is called phonon focusing, which means that the uniform angular distribution of wave vectors gives rise to a nonuniform distribution of group velocity vectors in an anisotropic medium and can be experimentally observed.[27]

Because of the anisotropic shapes of iso-energy surfaces, the $\theta\,(q,z)$ sectors are not the same as the $\theta\,(v,z)$ sectors in Fig. 7. As a result, figure 8 shows that there is significant difference in the contribution of CP thermal conductivity between the phonons in $\theta\,(q,z)$ sectors (dashed line with solid symbols) and those in $\theta\,(v,z)$ sectors (solid line with hollow symbols) at 300 K. The research about the wave vector angle $\theta\,(q,z)$ dependence shows that the relatively large contributions come from two sectors: $[0°, 15°)$ and $[60°, 75°)$, and the

contribution of ZO′ phonons increases with $\theta(q,z)$ increasing until a maximum value only about 8% in sector $[60°,75°)$ is reached.

Figure 8 reveals that phonons with group velocity close to CP direction and IP direction play an important role in CP thermal conduction. When the velocity vector angle $\theta(v,z) \in [0°,15°)$, the red arrows are distributed in a large part of BZ in the vicinity of Γ–A line, in which the largest wave vector angle $\theta(q,z)$ is about 45° for the ZA branch in Fig. 7(a), and about 60° for the ZO′ branch in Fig. 7(b). These phonons denoted by red arrows are apparently focused in the CP direction. When all branches are taken into account, the contribution (solid line with hollow dots in Fig. 8) due to phonons with $\theta(v,z) \in [0°,15°)$ has almost 44%, including 40% from the ZA phonons. If phonons with $\theta(v,z) \in [15°,30°)$ are also included, the total contribution will rise to 50%. By comparison, phonons with wave vector $\theta(q,z) \in [0°,15°)$ only transfer about 33% thermal energy in the CP direction, indicated by dashed line with solid dots in Fig. 8.

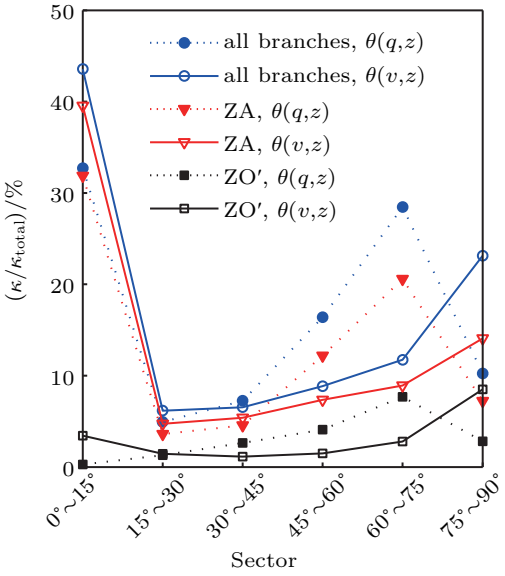


Fig. 8. CP thermal conductivity contributions at 300 K in $\theta(q,z)$ and $\theta(v,z)$ sectors defined in Fig. 7.

Phonons with blue arrows in Fig. 7 have group velocity vector angle $\theta(v,z) \in [75°,90°)$. A rough estimation tends to underestimate the contributions from these phonons. However, these blue arrows do have a component in the CP direction and the more important fact is that these phonons occupy at least 3/4 of BZ where phonon modes are distributed uniformly. When all the branches are considered, the contribution in $\theta(v,z) \in [75°,90°)$ is about 23%, including 14% from ZA phonons and 8% from ZO′ phonons.

Based on alamaBTE,[16] results can be given for each grid which represents a small part of BZ shown in Fig. 1. Therefore, the MFP projected in the CP direction for each mode $\{\Lambda_{pq}\}_c$ can be calculated. The largest value of $\{\Lambda_{pq}\}_c$ of ZA phonon and ZO′ phonon are found to be about 3 μm and 52 nm at 300 K. It is apparent that the transport properties of phonons can change dramatically and the MFP can span several orders of magnitude.[8] To assess MFP in a big picture view, the average MFP Λ_c defined in Eq. (4) is calculated, and the value is about 15 nm at 300 K, which is comparable to 20 nm estimated by Sadeghi *et al.* by using a theoretical method based on the full phonon dispersion.[7] The values of Λ_c are about 23 nm and 8 nm respectively for branch ZA and branch ZO′. It is apparent that the average MFP Λ_c is far lower than the maximum mode MFP $\{\Lambda_{pq}\}_c$. The reason is that as illustrated in Figs. 3 and 4, the ZA branch and ZO′ branch have the major contributions to CP thermal conduction, but have a small part of specific heat. Even for one branch, each different phonon mode has very significantly different $\{\Lambda_{pq}\}_c$. As a result, the average value calculated based on Eq. (4) is small.

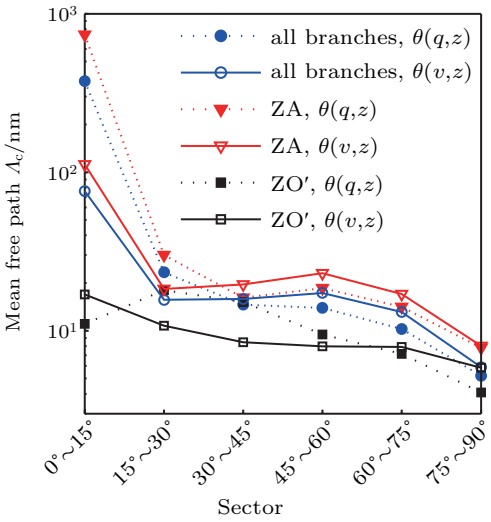


Fig. 9. Plots of average projected MFP at 300 K in CP direction in different sections defined according to angle $(\theta(q,z)$ or $\theta(v,z))$ range.

Figure 9 shows the plots of angle-dependent Λ_c at 300 K averaged in different sectors defined in Fig. 7. As discussed previously, ZO′ phonons have small contributions to CP thermal conduction. One reason revealed by Fig. 9 is that ZO′ phonons have Λ_c less than 20 nm in all the $\theta(q,z)$ sector (dashed line with solid squares) or $\theta(v,z)$ sectors (solid line with hollow squares). The dominant thermal energy carriers, ZA phonons that have long $\{\Lambda_{pq}\}_c$ are gathered around the Γ–A line. Therefore, the Λ_c value of all branches or ZA branch alone approximately tends to decrease as $\theta(q,z)$ or $\theta(v,z)$ increases. When the wave vector angle $\theta(q,z) \in [0°,15°)$, Λ_c of ZA branch denoted by dashed line with solid triangles has a large value of 737 nm. If all the branches are considered, Λ_c in sector $\theta(q,z) \in [0°,15°)$ decreases to 375 nm (dashed line with solid dots). When the group velocity angle $\theta(v,z) \in [0°,15°)$, the Λ_c of all branches (solid line with hollow circles) and ZA branch alone (solid line with hollow triangles) are 76 nm and 112 nm, respectively. As the longitudinal acoustic phonons, these ZA phonons with long Λ_c focus in the CP direction, their contribution to thermal conductivity is about 40% in $\theta(v,z) \in [0°,15°)$ as discussed previously in Fig. 8.

4. Conclusions

In summary, we have investigated the phonon transport along the CP direction of graphite from first-principles calculations and in the single-mode relaxation time approximation. The calculated phonon dispersion, CP thermal conductivity and specific heat for graphite are in good agreement with measurements. In a temperature range from 200 K to 1000 K, about 80% and 20% of contributions to CP heat transfer come respectively from ZA and ZO′ phonon branch, which are polarized in the CP direction, and can be regarded as longitudinal acoustic and optical branch for phonons with wave vectors along the Γ–A line in BZ, respectively. Except for ZA and ZO', the remaining phonon branches occupy most of thermal energy, but almost cannot transfer between graphite layers above 300 K. The phonons in the central 16% of BZ contribute 80% of CP transport. Phonons with group velocity angle $\theta(v,z)$ with respect to Γ–A less than 30° have 50% of CP transport at 300 K. The largest MFP in CP direction at 300 K is found to be about 3 μm and 52 nm for ZA and ZO′ phonon, respectively. The phonons with long MFP are gathered around Γ–A. When the group velocity angle $\theta(v,z) \in [0°, 15°)$, the average MFP in CP direction at 300 K for ZA branch is about 112 nm.

Acknowledgment

The author thanks Li Deyu for helpful discussion.

References

[1] Liu Y, Weiss N O, Duan X D, Cheng H C, Huang Y and Duan X F 2016 *Nat. Rev. Mater.* **1** 16042
[2] Yang J K, Yang Y, Waltermire S W, Wu X X, Zhang H T, Gutu T, Jiang Y F, Chen Y F, Zinn A A, Prasher R, Xu T T and Li D Y 2012 *Nat. Nanotechnol.* **7** 91
[3] Slack G A 1962 *Phys. Rev.* **127** 694
[4] Taylor R 1966 *Philos. Mag.* **13** 157
[5] Tanaka T and Suzuki H 1972 *Carbon* **10** 253
[6] Shen M, Schelling P K and Keblinski P 2013 *Phys. Rev. B* **88** 045444
[7] Sadeghi M M, Jo I and Shi L 2013 *Proc. Natl. Acad. Sci. USA* **110** 16321
[8] Wei Z Y, Yang J K, Chen W Y, Bi K D, Li D Y and Chen Y F 2014 *Appl. Phys. Lett.* **104** 081903
[9] Harb M, von Korff Schmising C, Enquist H, Jurgilaitis A, Maximov I, Shvets P V, Obraztsov A N, Khakhulin D, Wulff M and Larsson J 2012 *Appl. Phys. Lett.* **101** 233108
[10] Fu Q, Yang J K, Chen Y F, Li D Y and Xu D Y 2015 *Appl. Phys. Lett.* **106** 031905
[11] Zhang H, Chen X W, Jho Y D and Minnich A J 2016 *Nano Lett.* **16** 1643
[12] Minnich A J 2012 *Phys. Rev. Lett.* **109** 205901
[13] Yang F and Dames C 2013 *Phys. Rev. B* **87** 035437
[14] Yang J K, Shen M, Yang Y, Evans W J, Wei Z Y, Chen W Y, Zinn A A, Chen Y F, Prasher R, Xu T T, Keblinski P and Li D Y 2014 *Phys. Rev. Lett.* **112** 205901
[15] Han M, Liu J, Xie Y S and Wang X W 2018 *Carbon* **126** 532
[16] Carrete J, Vermeersch B, Katre A, van Roekeghem A, Wang T, Madsen G K H and Mingo N 2017 *Comput. Phys. Commun.* **220** 351
[17] Li W, Carrete J, Katcho N A and Mingo N 2014 *Comput. Phys. Commun.* **185** 1747
[18] http://www.almabte.eu/index.php/database/
[19] Mohr M, Maultzsch J, Dobardzic E, Reich S, Milosevic I, Damnjanovic M, Bosak A, Krisch M and Thomsen C 2007 *Phys. Rev. B* **76** 035439
[20] Maultzsch J, Reich S, Thomsen C, Requardt H and Ordejon P 2004 *Phys. Rev. Lett.* **92** 075501
[21] Nicklow R, Wakabayashi N and Smith H G 1972 *Phys. Rev. B* **5** 4951
[22] Paulatto L, Mauri F and Lazzeri M 2013 *Phys. Rev. B* **87** 214303
[23] Hazrati E, de Wijs G A and Brocks G 2014 *Phys. Rev. B* **90** 155448
[24] Ho C Y, Powell R W and Liley P E 1972 *J. Phys. Chem. Ref. Data* **1** 279
[25] Incropera F P, Bergman T L, Lavine A S and Dewitt D P 2011 *Fundamentals of heat and mass transfer*, 7th edn. (USA: John Wiley & Sons, Inc.) p. 987
[26] Ziman J M 1960 *Electrons and Phonons* (Oxford: Clarendon Press) p. 48
[27] Wolfe J P 1998 *Imaging phonons: acoustic wave propagation in solids* (New York: Cambridge University Press) p. 60